Prelim Rough Draft I

Julien Varennes

January 5, 2016

1 Introduction

1.1 What is the problem?

The largest cause of death in cancer patients is due to the onset of metastasis. The first step in metastasis is invasion of tumor cells into the surrounding micro-environment. Invasion is known to occur in a highly organized manner [1]. Recent work shows that tumor cell invasion is guided by sensory cues to blood vessels and to lymphatics [2], and that cancer cells can sense their environment with remarkable precision. Studies on breast cancer show that environmental signaling is used by invasive tumor cells. Utilizing interstitial flow, breast tumor cells chemotax to the draining lymphatic by sensing chemical gradients [2]. It is clear that the early stages of metastasis depend on cell sensing, hence understanding how the limits of cell sensing affect collective cell migration can help us better understand how collective invasion occurs.

1.2 What is the gap in knowledge?

The gap is the missing link between the collective sensing process cells use and the mechanical behavior of cell migration. Cells measure their environment, share that measurement with other cells, and then apply that information to the cell's behavior (in this case the behavior of interest is migration).

Cells are known to interact with surrounding cells. Cells can act collectively and in some cases this is mediated via intercellular communication. Work has been done on developing predictions on the limits of collective cell sensing. Collectives of cells sense their local environment and share that information with neighboring cells in order to increase the accuracy of their measurements. Collective groups of cells are also observed to behave in a coordinated, and organized fashion in certain situations. Specifically, cell migration is observed to occur in collective groups in many instances.

It is natural to ponder the connection between these two characteristics of cell collectives. Collective groups of cells use communication in order to enhance the accuracy of their sensing. This feature may play a role in the collective migration process. Therefore, the gap that I want to address is the missing connection between collective cell sensing and collective cell migration.

1.3 How will my research address the gap in knowledge?

My research will address this gap by developing a model that connects multicell sensing with collective migration. The model composes of a multicellular sensing model in which cells can sense chemical concentrations and gradients in their surrounding environment. The output of this sensing process is then coupled to cell dynamics in order to produce migratory behavior.

I will develop of computational implementation of the model in order to understand what it is capable of. Using computer simulations, relationships between parameters in the model can be obtained numerically. The simulation will be capable of simulating 2D systems of cells.

In conjunction with the development and analysis of numerical simulations I will work with experimental collaborators and verify whether my model can indeed reproduce experimental results. The experiments performed by Professor Han and his students will observe if/how breast cancer cells migrate in the presence of a chemical concentration. Using my numerical simulations I can predict optimal cell cluster size for most efficient migration.

The third project is still under development. One idea is to develop a different model to see if there are alternative methods which cells may use in order to produce collective, coordinated behavior. Another idea is to see how EMT affects cell migration.

1.4 How will I know I am finished?

I will know that my model is complete when I have explored the different behavior the model does in different parameter regimes. The model should produce the desired collective migratory behavior for a robust range of parameters. The model should breakdown for extreme parameter regimes. Using numerical simulations I should be able to characterize the relationship on mean first passage time (mFPT) and the model parameters. Determine an optimal number of cells for fastest collective migration.

I will know I am done with the collaborative research project when we successfully characterized the experimental observations. Model parameters are successfully matched with biological/experiemental parameters and observables. Numerical simulations can qualitatively replicate experimental behavior. The model can predict experimental measurable results accurately.

2 Thesis Plan

2.1 Collective Cell Sensing and Migration Model

The goal of this project is to describe and quantify intercellular communication and multicellular migration. Collective sensing can improve cell's ability to sense the environment, and in turn this information is used in directing the cell's behavior. However, there lacks a model to explain how collective sensing in facts affects a cell's behavior. In my research I will focus my attention on how collective sensing connects with multicellular migration. Before developing a model of collective sensing and migration we must first learn about present theories and models of sensing and migration.

2.2 Application of the Collective Sensing and Migration Model

In conjunction with the development and analysis of numerical simulations I will work with experimental collaborators in Prof. Bumsoo Han and his group, in order to verify whether my model can indeed reproduce experimental results. The experiments performed by Prof. Han and his group will observe how breast cancer cells migrate in the presence of a chemical concentration. Using the previously developed numerical simulations an optimal cell cluster size for most efficient migration can be predicted and compared to experimental findings.

In addition to working in collaboration on breast cancer cell migration, the model can be further applied to systems of cells of different phenotypes. It is known that invasive cell clusters have leading-edge cells that are phenotypically different than the trailing cell in the cluster [3].

Add more citations. With some slight modifications, the simulations can be used to predict how leader cells may behave within a cluster of communicating cells.

2.3 Many Wrongs Method of Cell Migration

Another interesting way for collective behavior can emerge through individual sensing and migration. In this sort of model, single cells independently sense gradients and migrate, although it may at lower precision than the case of the collective sensing model. When many cells are located near one another, the group migration can become directed through local interaction between cells. Even though each cell has low sensory and migratory accuracy, the precision of the group as whole is increased due to local interactions. This mechanism is termed the "many wrongs" model and it has been shown the group migratory behavior can emerge from this model [4, 5]. Local interactions act to average over the errors in individual cell sensing, thereby decoupling group behavior from single-cell properties. This part of the project will aim to verify whether or not intercelllular communication is the best way to achieve collective migration or not.

3 Preliminary Results

3.1 Modelling Collective Sensing

Multicellular communication can prove very useful is enhancing cell sensing. For example, in many types of cancer tumor cell invasion is a multicellular process and so multcell communication and sensing may be at work [3, 1]. In the case of extremely shallow gradients, groups of cells can sense gradients that individual cells cannot. Experiments have shown this to be true in the case of mammary epithelial cells [6]. Cells in different systems are communicating with one another and it clearly can be very advantageous to do so.

3.1.1 Sensing, Background Information

Before we discuss multicellular communication and sensing in the context of my model, it is important to know how cells may sense their environment and the physical limits to their sensing.

Limits to the precision of single-cell concentration sensing were first derived by Berg and Purcell almost 40 years ago[7]. In their study, Berg and Purcell first considered a cell acting as a perfect counting instrument. In this simplest of models, the cell is a sphere of diameter a and volume V through which molecules can freely diffuse in and out. Assuming that the molecule concentration is uniform, and that the cell derives all its information about the concentration by counting each molecule inside its spherical body, the expected count is $\bar{n} = \bar{c}V$ where $\bar{c}$ is the mean concentration. Since diffusion is a Poisson process the number of molecules the cell counts will fluctuate around the expected value $\bar{n}$. It is known that for a Poisson process the variance σ_n^2 is equal to the mean $\bar{n}$, and therefore the relative error in the cell's concentration estimate is $\sigma_c/\bar{c} = \sigma_n/\bar{n} = 1/\sqrt{\bar{c}V}$.

The cell can decrease its relative error by taking several measurements of the molecules inside it and time-averaging the results. However, individual measurements must be separated by a sufficient amount so that the molecules inside the cell are refreshed. The time-scale for this is characterized by the diffusion time, $\tau \sim V^{2/3}/D \sim a^2/D$, where D is the diffusion constant. Assuming the cell integrates over a time period T, the cell makes $\nu = T/\tau$ independent measurements thus reducing the variance by a factor of $1/\nu$. This gives the long-standing lower

limit on the relative error in single-cell concentration sensing

$$\frac{\sigma_c}{\bar{c}} = \frac{\sigma_n}{\bar{n}} \sim \frac{1}{\sqrt{a\bar{c}DT}}. \tag{1}$$

The relative error decreases with increased cell size (a) and chemical concentration ($\bar{c}$), since this increases $\bar{n}$. Being able to take more independent measurements benefits the cell, hence with increasing D and T the relative error goes down. This limit has been more rigorously derived [7] and the effects of binding kinetics, spatial confinement and, spatiotemporal correlations have also been studied [8, 9, 10]. Nonetheless, a term of the form in Eq. 1 emerges in all cases as the fundamental limit for single-cell concentration sensing.

These simple limits to concentration sensing can be extended single-cell gradient sensing. One simple, common way for cells to measure a chemical concentration gradient is to compare concentration measurements made at different locations along the cell body [11]. We treat these compartments as idealized counting volumes as done for previously however, in reality these compartments are usually receptors or groups of receptors on the cell surface. The cell can estimate the chemical gradient by taking the difference in counts between two such compartments.

Consider two compartments of size s that are located on opposite ends of a cell of diameter a. Let a chemical gradient $\bar{g}$ run parallel to the compartments, each compartment on average will measure chemical concentrations $\bar{c}_1$ and $\bar{c}_2 = \bar{c}_1 + a\bar{g}$, respectively. This corresponds to average molecule counts that are approximately $\bar{n}_1 = s^3\bar{c}_1$ and $\bar{n}_2 = s^3\bar{c}_2$. Assuming that the measurements made in each compartment are independent, then the difference in counts is proportional to the gradient $\Delta\bar{n} = \bar{n}_2 - \bar{n}_1 = as^3\bar{g}$. Using Eq. 1 we find the variance in the difference to be $\sigma^2_{\Delta n} = \sigma^2_{n_1} + \sigma^2_{n_2} \sim \bar{n}_1^2/(s\bar{c}_1DT) + \bar{n}_2^2/(s\bar{c}_2DT)$. This limit can be further simplified by assuming that the gradient is very small relative to the concentration $a\bar{g} \ll \bar{c}_1$, resulting in $\bar{c}_1 \approx \bar{c}_2 \approx \bar{c}$ the concentration at the center of the cell and so $\sigma^2_{\Delta n} \sim (s^3\bar{c})^2/(s\bar{c}DT)$ where the factor of 2 is neglected in this simple scaling estimate. Thus the relative error in gradient sensing simplifies to

$$\frac{\sigma_g}{\bar{g}} = \frac{\sigma_{\Delta n}}{\Delta\bar{n}} \sim \sqrt{\frac{\bar{c}}{s(a\bar{g})^2DT}}. \tag{2}$$

Similar to Eq. 1, the relative error decreases with compartment size s, and also with D and T. The relative error decreases with $a\bar{g}$ because the measurements made by the two compartments are more different from each other. Unlike concentration sensing, the relative error for gradient sensing increases with $\bar{c}$ because it is more difficult to measure a small difference in concentration on a larger background than on a smaller one [6]. Eq. 2 has been more extensively derived and generalized to systems with compartments of different geometries [12, 13, 14]. In all such cases a term of the form in Eq. 2 appears as the fundamental limit, with the length-scale s dictated by the particular sensory mechanism and geometry.

It is clear from Eq. 2 that multicellular collective can more accurately detect gradients than a single cell since a collective of cells can span a larger region of the chemical gradient. If we consider the cells opposite ends of the cluster as the two compartments comparing concentration measurements, then in Eq. 2 $s \to a$ and $a \to Na$ where N is the number of cells running parallel to the gradient. The relative error for the multicellular cluster becomes [15]

$$\frac{\sigma_g}{\bar{g}} \sim \sqrt{\frac{\bar{c}}{a(Na\bar{g})^2DT}}. \tag{3}$$

However, there is a crucial effect that was neglected in formulating Eq. 3 which is the mechanism by which the cells communicate their measurements across the cluster. This will introduce additional noise to the gradient sensing process thereby altering the expression for the relative

error. In the case of a single cell it is reasonable to assume that measurements from different compartments can be reliably transmitted, but with the increased size of the multicellular cluster we can no longer neglect this effect. The physical limits to communication-aided collective gradient sensing have been derived [6, 15]. In these studies the local excitation–global inhibition (LEGI) paradigm [16] to model inter-cell communication. The LEGI paradigm is one of the simplest ways to model adaptive, multicellular sensing. In the model cells produce both a "local" and a "global" molecular species in response to the chemoattractant, and the global species provides the communication by diffusing between neighboring cells. The difference between local and global molecule numbers in a given cell provides the readout. A positive difference informs the cell that its measurement is above the spatial average among its neighbors, and therefore that the cell is located up the gradient, not down. The relative error of gradient sensing was found to be limited from below by

$$\frac{\sigma_g}{\bar{g}} \sim \sqrt{\frac{\bar{c}}{a(n_0 a\bar{g})^2 DT}}, \tag{4}$$

where n_0^2 is the ratio of the cell-cell exchange rate to the degradation rate of the global species. This parameter sets an effective length-scale $n_0 a$ over which cells can reliably share information. Therefore, as the cell collective grows larger than n_0 cells the relative error does not improve, unlike Eq. 3 where the effects of communication are ignored.

3.2 Sensing, Implementation

In our model, multicellular sensing of noisy chemical gradients is modeled using the LEGI paradigm [15, 16]. The LEGI model is the simplest model of gradient sensing that is adaptive to changes in concentration, and so gradient detection can be made independent of the background concentration. Adaptation of intercellular communication is experimentally motivated. Gain factors can be easily implemented using LEGI which is important if downstream amplification is desired.

In the simulations, cells produce two chemical species, X and Y, in response to the chemical concentration of S in the environment. The local reporter species X remains within individual cells and represents that cell's measurement of its local chemical concentration whereas the global reporter Y that can diffuse at the rate γ between adjoining cells. The chemical reactions are illustrated below.

$$\begin{aligned} S &\to S + X \qquad X \to R \\ S &\to S + Y \qquad Y \dashv R \end{aligned}$$

$$\begin{aligned} s_k &\xrightarrow{\kappa} s_k + x_k \qquad x_k \xrightarrow{\mu} \emptyset \qquad y_k \underset{\gamma_{j,k}}{\overset{\gamma_{k,j}}{\rightleftharpoons}} y_j \\ s_k &\xrightarrow{\kappa} s_k + y_k \qquad y_k \xrightarrow{\mu} \emptyset \end{aligned} \tag{5}$$

The global reporter molecules exchange rate is dependent on the size of the contact made between adjacent cell.

$$\gamma_{j,k} = \int_{\mathcal{C}} \Gamma dl \tag{6}$$

$$R_k = x_k - y_k \tag{7}$$

Individual cells can then check whether or not they are above or below the global average via the downstream readout species R. A negative (positive) difference tells the cells it's below (above) the average. The chemical concentration is modeled as a space-dependent field, and in this case has a constant gradient in the x-direction.

$$E(x,y) = gx + g_0$$
$$[E] = \text{molecules/area}$$

The average signal around the cell is $\bar{s}_k = \int_k dA\ E(x,y)$. Since diffusion is a Poisson process the variance in the measured signal s_k is equal to the mean, so $\sigma^2_{s_k} = \bar{s}_k$. The dynamics of the local reporter satisfy the stochastic equation

$$\dot{x}_k = \kappa s_k - \mu x_k + \eta_{x_k} \tag{8}$$
$$\eta_{x_k} = \sqrt{\kappa \bar{s}_k}\xi_2 - \sqrt{\mu \bar{x}_k}\xi_3$$

In Eq 8 and subsequent stochastic equations ξ_i and $\chi_{j,k}$ are unit Gaussian random variables that simulate the noise in the molecule population. The dynamics of the global species can be modeled in similar fashion.

$$\dot{y}_k = \kappa s_k - \mu y_k - y_k \sum_{<j,k>} \gamma_{j,k} + \sum_{<j,k>} y_j\ \gamma_{j,k} + \eta_{y_k} \tag{9}$$

$$\eta_{y_k} = \sqrt{\kappa \bar{s}_k}\xi_4 - \sqrt{mu\bar{y}_k}\xi_5 + \sum_{j=1}^{N} \left[\chi_{j,k}\sqrt{\gamma_{j,k}}\left(\sqrt{\bar{y}_j} - \sqrt{\bar{y}_k}\right)\right]$$

The first summation term accounts for the loss of y_k due to the diffusion into neighboring cells, and similarly the second summation term accounts for the increase in y_k due to diffusion into cell k from neighboring cells. The notation $< j,k >$ represents all nearest neighbor pairs. This expression can be simplified by noting $\gamma_{j,k} = \gamma_{k,j}$, $\gamma_{i,i} = 0$, and defining the sum of all the exchange rates between cell k and all other cells $\Gamma_k = \sum_{j=1}^{N} \gamma_{j,k}$.

For the local reporter, the steady-state solution is simply

$$x_k^{ss} = (\kappa/\mu)\, s_k + (1/\mu)\, \eta_{x_k}. \tag{10}$$

The steady-state solution for the global reporter is more involved, and can be written as a matrix equation $M\vec{y}^{ss} = \kappa\vec{s} + \vec{\eta}_y$ where M is a square, symmetric matrix that governs the degradation and exchange y in all cells.

$$M = \begin{bmatrix} \mu + \Gamma_1 & -\gamma_{1,2} & \cdots & -\gamma_{1,N} \\ -\gamma_{2,1} & \mu + \Gamma_2 & \cdots & -\gamma_{2,N} \\ \vdots & \vdots & \ddots & \vdots \\ -\gamma_{N,1} & -\gamma_{N,2} & \cdots & \mu + \Gamma_N \end{bmatrix} \tag{11}$$

In simulations, Eq. 11 is solved numerically for $\vec{y}^{ss}$ the vector of global molecule population in every cell.

Check the η_{y_k} equation, check vector equation if the vector is for $\bar{s}$ values or s. Add a picture as proof of concept of signaling (like 2 cell example from posters).

We can calculate the error in the system by

3.3 Modelling Collective Migration

The next step in our study is to connect collective migration with multicellular sensing. Modeling cellular migration is an interesting problem because often rich and sophisticated behavior can emerge from a few interaction rules. Even in the absence of sensing, simple models are successful at explaining observed collective behaviors such as cell streaming, cell sorting, cell sheet migration, wound healing, and cell aggregation [17, 18, 19, 20]. These models are very interesting and have myriad applications but they ignore the cell's sensing capabilities and its potential ramifications on cell behavior.

Recently, Camely et. al. developed a model in order to connect cell sensing and multicellular chemotaxis [21]. In this model, cells are tightly connected but are polarized away from neighboring cells due to contact inhibition of locomotion (CIL), the physical phenomenon of cells ceasing motion in the direction of cell-cell contact [22]. Individual cells sense the local chemoattractant concentration and are polarized with a strength proportional to this concentration but, the mechanical coupling acts to keep them together. In the presence of a concentration gradient, the difference in individual cell's measurements causes an imbalance in migration strengths resulting in net directed motion and successful chemotaxis. This model is very interesting since cell clusters chemotax even though individual cells cannot, since without other cells, there is no CIL to bias the direction of motion. Although this is a very valuable model it has its shortcomings. Firstly it does not deal naturally account for the stochastic nature of cellular behavior, instead a noise term is tacked onto the dynamics. Secondly, cell to cell communication is not addressed, and although it is not the aim of that paper to do so, it does leave us without a model suitable to our interests.

From looking through the literature we have seen that modeling collective cellular behavior is an active field of research. Indeed, many models exist that are able to characterize collective behavior of cells. There are also models that take into account cell sensing and how it affects cell dynamics [5, 21]. However, there is a lack of models which combine the effects of multicellular communication with collective cellular migration. We will use our lessons learned from the literature in order to develop such a model.

3.4 Sensing-Coupled Cell Dynamics

The information gained from multicellular sensing is then used to influence cell dynamics by coupling R to individual cell polarization $\vec{p}$. Modeling collective behavior using cell polarization has been used in the past [18, 21]. In order for clusters of cells to achieve migration in the direction of increasing chemical concentration individual cell polarization vectors should be dependent on the cell's location within the cluster. Information of about the cell's surroundings are naturally expressed by a cell repulsion vector $\vec{q}$ [21]. The repulsion vector for cell k is a unit vector that points away from all of cell k's neighbors.

$$\vec{q}_k = \left(\frac{1}{\sum_{<j,k>} L_{j,k} |\vec{x}_k - \vec{x}_j|} \right) \sum_{<j,k>} L_{j,k} \left(\vec{x}_k - \vec{x}_j \right) \tag{12}$$

$L_{j,k}$ is the contact length made between cell k and it's neighbor cell j. The repulsion vector is representative of contact inhibited locomotion (CIL). CIL may decrease motility in the direction of the contact and shows that cells are aware of their immediate surroundings. Using a combination of the repulsion vector and the downstream readout the cell's polarization will change.

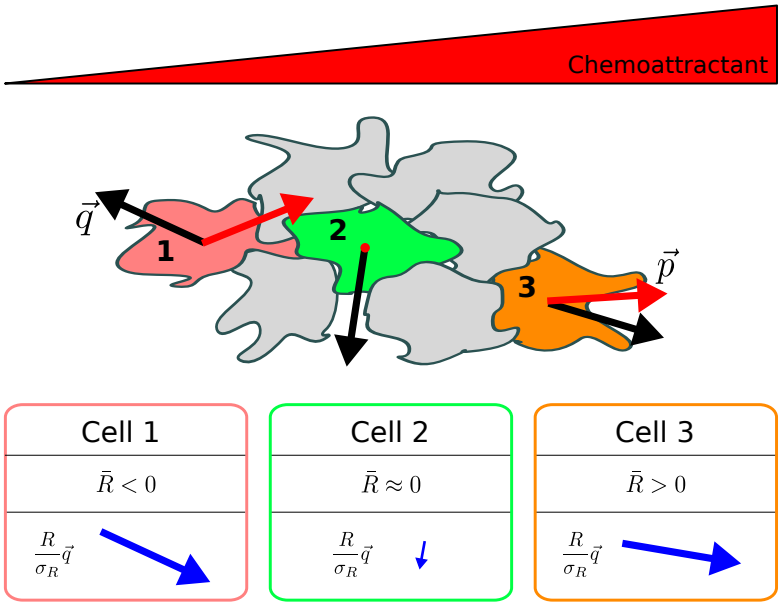

Figure 1: Cell polarization is biased by multicellular sensing. The downstream read-out R of the LEGI model is dependent on the cell's location within the cluster. Cells on the left & right edges will tend to move in the direction of the gradient, while cells in the middle are on average not polarized. Polarization vectors $\vec{p}$ are red, repulsion vectors $\vec{q}$ are black. The effect of sensing on cell polarization is represented by the blue arrows.

$$\frac{d\vec{p}_k}{dt} = r\left[-\vec{p}_k + \epsilon\frac{R_k}{\sigma_R}\vec{q}_k\right] \tag{13}$$

The first term represents the decay of the polarization vector. In the absence of a chemical concentration an individual cell will undergo a persistent random walk; the cell's direction changes at a rate r. The second term acts to align or anti-align the cell's polarization vector with the repulsion vector based on the cell's information about the chemical gradient encoded in R. The net effect is illustrated in figure.

In this model clusters of multiple cells can successfully chemotax in the direction of increasing chemical concentration. It is important to note that this model fails in the case of single cell chemotaxis and is only relevant to systems of multi-cell migration. Single cells are not able to detect gradients on their own and similarly without neighboring cells there is no repulsion vector to influence the cell's polarization.

3.5 Computational Implementation

A computational implementation is required in order to understand the dynamics that evolve from the model of collective sensing and migration. Simulations are an essential way to characterize the types of behaviors the model produces along with comparing those with experiment. The implementation chosen is the Cellular Potts Model (CPM). CPM is widely used for simulating cell-centric systems. Despite their simplicity these models can qualitatively reproduce diverse biological phenomena [23, 24, 25]. The CPM is a very good implementation for simulating systems wherein cell geometry is crucial to the dynamics of the system. CPM has been used

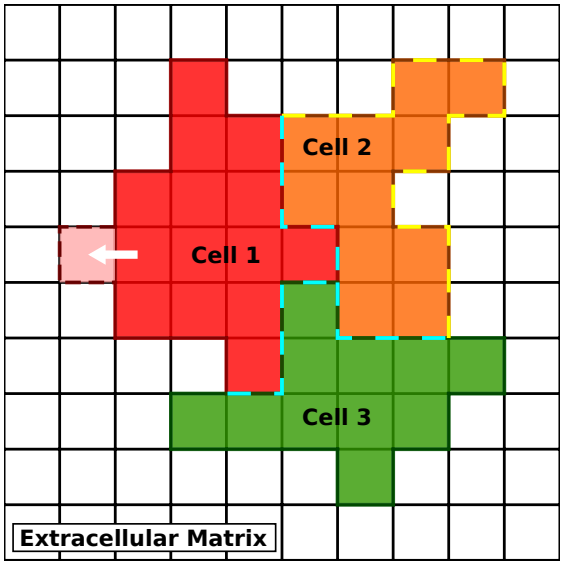

Figure 2: Illustration of the Cellular Potts Model (CPM). Cells comprise of simply connected lattice points. There are adhesion energies associated with different types of contact: cell-cell (blue-dashed line), and cell-ECM (yellow-dashed line). Cell motility is modeled by the addition/removal of lattice points (pink).

to simulate models describing cell sorting, streaming, and chemotaxis [26]. Using CPM, models involving cell polarization and mechanical-based coupling successfully reproduce epithelial cell streaming, cell sorting, and collective migration [17, 18].

In the CPM model cells live on a discrete lattice and are represented as groupings of lattice points. Simply-connected groups of lattice sites x with the same integer values for the *lattice label* $\sigma(x) > 0$ comprise a single cell. The extracellular matrix (ECM) is labeled with $\sigma(x) = 0$. Cells have a desired size and circumference from which they can fluctuate. Cells adhere to their neighbors with an associated adhesion energy. The energy of the whole system is the sum of contributions from adhesion $J_{i,j}$, area-restriction λ_A, and circumference-restriction λ_P terms.

$$U = \sum_{<x,x'>} J_{\sigma(x),\sigma(x')} + \sum_{i=1}^{N} \left(\lambda_A(\delta A_i)^2 + \lambda_P(\delta P_i)^2\right) \tag{14}$$

$$J_{\sigma(x),\sigma(x')} = \begin{cases} 0, & \sigma(x) = \sigma(x') \text{ (within the same cell)} \\ \alpha, & \sigma(x)\sigma(x') > 0 \text{ (cell-cell contact)} \\ \beta, & \sigma(x)\sigma(x') = 0 \text{ (cell-ECM contact)} \end{cases} \tag{15}$$

The parameters α and β characterize intercellular adhesiveness. In order to ensure that it is energetically favorable for cells to remain in contact with one another $\beta > 2\alpha$ [18]. The volume and circumference-restriction energy terms restrict cells from growing or shrinking to unphysical sizes as well as branching or stretching into unphysical shapes. Cells fluctuate in shape and size around the desired size A_0 and circumference P_0 with $\delta A_i \equiv A_i - A_0$ (and similarly for δP_i). The resulting dynamics evolve from the minimization of the system's energy under thermal fluctuations.

Cell dynamics are a consequence of minimizing the energy of the whole system. This is a random process that is sensitive to thermal fluctuations and is modeled using a Monte Carlo process. In a system of n latice sites, one *Monte Carlo* time step (MC step) is composed of n *elementary* steps. Each elementary step comprises of an attempt to copy the lattice label of a randomly chosen lattice site onto that of a randomly chosen neighbor. The new configuration resulting from the copy is accepted with probability P, which depends on the change in the system's energy accrued in copying over the lattice label.

$$P = \begin{cases} e^{-(\Delta u - w)}, & \Delta U - w > 0 \\ 1, & \Delta U - w < 0 \end{cases} \tag{16}$$

The term Δu is the change in energy of the system due to the proposed lattice label copy. w is the *bias* term which acts to bias cell motion in the direction of polarization. The bias term in the CPM model is required in order for cell clusters to exhibit collective directed migration.

$$w = \sum_{k=\sigma(a),\sigma(b)} \frac{\Delta\vec{x}_{k(a\to b)} \cdot \vec{p}_k}{|\Delta\vec{x}_{k(a\to b)}||\Delta\vec{x}_{k(\Delta t)}|} \tag{17}$$

The summation is over the cells involved in the elementary time step. The change in the cell's center of mass position during the elementary time step is $\Delta\vec{x}_{k(a\to b)}$, whereas $\Delta\vec{x}_{k(\Delta t)}$ is the cell's change in center of mass during a MC step. The cell polarization vector $\vec{p}_k$ is updated at every MC step in accordance with equation (13). The dot product acts to bias cell motion since movement that is parallel to the polarization vector will result in a more positive w which in turn results in a higher acceptance probability.

The dynamics that evolve from the computer simulations are in agreement with those outlined in the model. As illustrated in figure 1, using this computational implementation leads to cell's on the edges of the cluster being polarized in the direction of increasing chemical concentration, and leaves cells in the center with no net polarization.

3.6 Collective Sensing and Migration: Preliminary Results

Using our simulations we can calculate statistics on multicellular migration and sensing. One such statistic is the first-passage time which is the time it takes for a cluster of cells to travel a fixed distance; the threshold distance is measured with respect to the cluster center of mass.

Since the simulations represent stochastic processes it is important to run several instances and gather statistics on the first-passage time. Before we begin to investigate how well communicating clusters of cells perform it is important to understand the effects of the various parameters on our simulations. From examining the simulated cell behavior for different parameter values we identify two crucial parameters: β the cell-ECM adhesion energy, and ϵ the polarization bias strength. When we vary these two parameters we find three distinct phases of cell migration.

We see that in the center of the figure the mean first-passage time (MFPT) remains relatively constant as β and ϵ grow in proportion to one another. In this phase, the clusters of behaving as desired. However if the adhesion energy is increased further while the bias strength remains fixed the MFPT starts to increase. This is due to the increased energy cost in cells making protrusions into the ECM. If β is increased further the cluster cells will eventually stop moving since protrusions are nearly impossible to achieve. The other large MFPT phase is due to increasing ϵ while keeping β fixed. In this case the cell's polarization becomes large enough to overcome the intercell adhesion energy causing the cluster of cells to scatter. When the cells are not in contact they cannot measure the chemical concentration and their motion becomes unbiased. Therefore there is a large region in parameter space where the simulated is physically

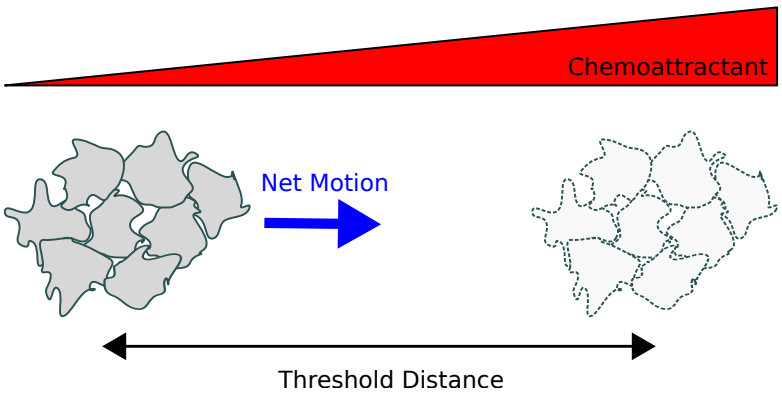

Figure 3: A first-passage time process. The first-passage time is the time it takes for the center of mass of the cell cluster to reach a threshold distance.

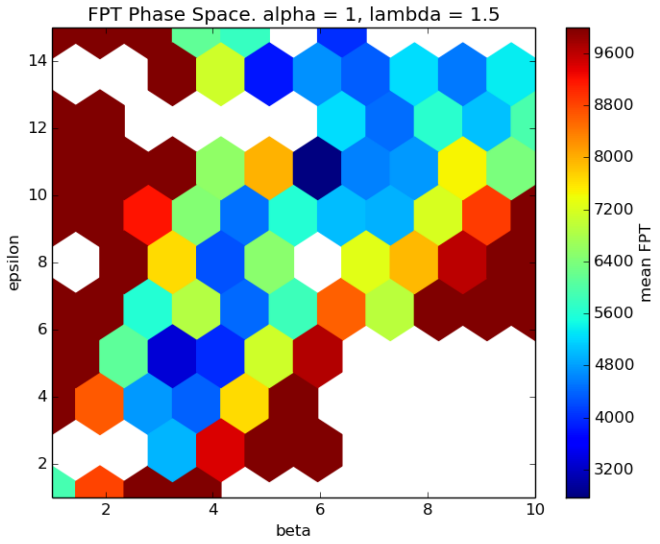

Figure 4: A heatmap of mean first-passage times (MFPT) as a function of β (cell-ECM adhesion energy), and ϵ (polarization bias strength). Warm colors represent large MFPT valuess.

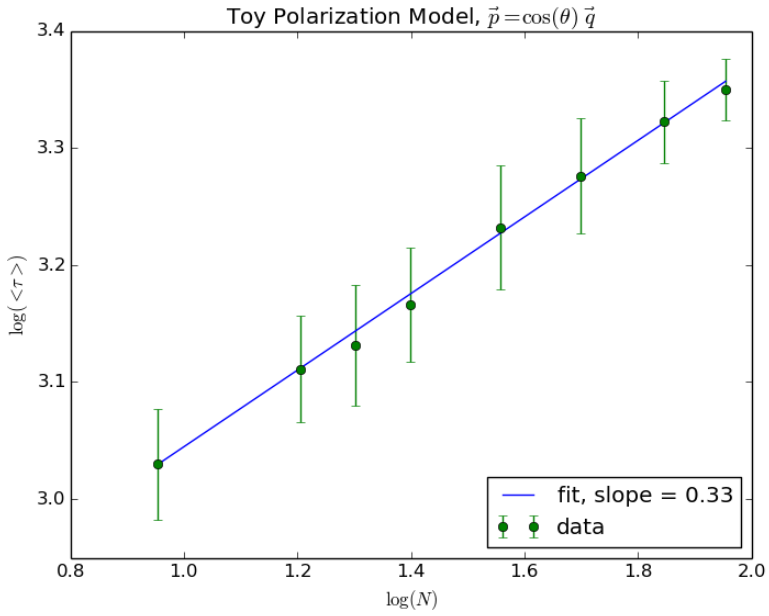

Figure 5: First-passage times for the simplified migration model for cluster of various number of cells.

realistic and in the limits where we would expect our model to breakdown the simulations do as well.

With this in mind we can examine the MFPT as a function of the number of cells in a cluster for reasonable parameter values β and ϵ. For the

3.6.1 Seperating Migration from Sensing

In analysing simulation results it is important to understand the relationship between cell cluster size and firt-passage time. In order to simplify the problem it is useful to separate the effects of sensing from those purely due to the mechanics of migration. In the limit of perfect sensing cluster migration essentially becomes independent from the sensing mechanism since the cells perfectly measure the gradient. The cells located on the edge of the cluster on where $R > 0$ will have polarization vectors that point out from the cluster, whereas cells on the opposite side where $R < 0$ will have their polarization vectors pointing inward. With this simplified migration model we can study how first-passage times scale with the cluster size.

As shown in Fig. 5, we find a power-law relationship between the number of cells N and the mean first-passage time $< \tau >$. This relationship can be understood through simple scaling arguments on the drag and driving forces on the cluster. The first-passage time should scale proportionally with the drag experienced on the cluster, whereas it should be inversely related to the force driving migration.

$$< \tau > \sim \frac{\text{drag}}{\text{force}} \tag{18}$$

The drag on the cluster will increase with the size of the cluster drag $\propto A(N)$, and the driving force should scale with the perimeter of the cluster since we know that only cells on the edges of the cluster will be polarized in the desired direction, force $\propto P(N)$. From simulations we

can see the functional relationship of the area $A(N)$ and the perimeter $P(N)$ on the number of cells within the cluster. As expected the area of the cluster grows with the number of cells $A(N) \sim N$. Interestingly, the perimeter of the cluster scales as $P(N) \sim N^{0.63}$ which tells us that the preferred cluster geometry is more amoeboid than circular. Plugging this into Eq. 18 we find that $< \tau > \sim N^{0.37}$ which is in agreement with the simulation results. Therefore, the migratory behavior can be understood purely from the goemetry of the cluster.

Add figures of $A(N)$, $P(N)$ scaling. Maybe combine them with Fig. 5. Also add diagram illustrating toy FPT model.

Next, we examine the MFPT results for the complete, collective sensing and migration model. Starting from $N = 2$ we see that as the number of cells increases the MFPT decreases; this can be understood from our understanding of multicellular sensing. Before reaching the limiting length-scale $n_0 a$ the error in sensing decreases as $1/N^2$ and so the cluster's ability to correctly sense the gradient and thus migrate in the correct direction increases. However, MFPT reaches a minimum around $N \sim 20$ cells after which the MFPT no longer improves. There are two effects that contribute to the MFPT reaching a minimum: one is the increased drag caused by adding additional cells, as observed earlier, in the absence of sensing the MFPT will continually increase as the cluster grows in size. Second is the reduced benefit to sensory precision with larger clusters, once the critical length-scale spans the gradient sensing cannot become any better.

4 Applications of the Collective Sensing and Migration Model

4.1 Cancer Cell Migration Collaborative Research

The goal of this part of the thesis is to apply the model of collective cell sensing and migration to breast cancer cell migration experiments. By collaborating with Prof. Bumsoo Han and his group it is possible to develop an integrated mathematical and experimental model of collective tumor cell invasion. Previous experiments have shown that tumor cells invade as collective aggregates [3, 1]. In applying the model to tumor cell invasion we can quantify the degree with which invasion is aided by collective communication.

Experiments on breast cancer cell clusters of varying size will be done in order to determine invasiveness depends on cluster size. Clusters of cells will be placed in a microfluidic device [27, 28] in which cells are exposed to concentration gradients of known breast cancer attractors. Collective migration of the cells into the surrounding collagen will be the measured in order to quantify the potential invasiveness of the clusters.

The experimental set-up will be reproduced computationally in order to see whether the model can predict the observed behavior. Working in conjunction with experiments will be very helpful in refining the model for the application of tumor cell invasion and understanding the relationship between model parameters and experimental behavior. The model will be able to predict which cluster size(s) exhibits the most efficient collective migration under experimentally determined chemical gradients. Therefore, our collaboration will be able to predict and quantify which cluster size(s) has the highest invasive potential.

The experimental device is composed of three sections. The central section comprises the collogen matrix in which cells are placed. The central section is neighbored on either side by channels which can have fluid flowing through them. For this project, one channel will have a chemoattractant culture flowing through it whereas the other will be chemoattractant-free culture medium. The different fluids flowing through either channel causes a gradient in chemoattractant concentration across the central, collagen hydrogel.

	Experiment	Simulation
Length	1μm	0.4px
Chemical Concentration	1nM	9.4molecules/px^3
Concentration Gradient	1nM/mm	0.02molecules/px^4

Table 1: Conversion of physical units to computer simulation units.

The current state of the experiments are that clusters of cells of variable size can be cultured in the hydrogel and cells can be counted. Bumsoo's group is able to image and track individual cells by recording the location of their centroids. Gradients of growth factor can be formed successfully across the gel.

4.1.1 Unit Comparison

Even without experimental data we can still make comparisons between physical experiments and numerical simulations. From experiments on culturing the cells in the hydrogel cell sizes can by compared between experiment and simulation. Experiments report that cell's have a radius of $r \approx 10\mu$m. In our simulation cells have a target size $A_0 = 50\text{px}^2$ where px is the length of one simulation lattice site. Setting the simulation target area equal to that seen in experiment we find that $1\text{px} = 2.5\mu$m. With this information we can also convert chemical concentrations to and from simulation units, $9.4 \cdot 10^9 \frac{\text{molecules}}{\text{px}^3} = 1\text{M}$. More simply stated, 1nM is equivalent to about 9molecules/px^3. The various conversions that can be derived are listed in Table 1.

Using these conversions we are able to model extremely small chemical concentrations and gradients, which approach the theoretical limits of collective sensing. From simulations we see that cell clusters in the model can successfully chemotax. It is yet to be seen whether these findings may be replicated in experiment.

5 Thesis Part 3. Collective Migration via Many Wrongs

References

[1] Peter Friedl, Joseph Locker, Erik Sahai, and Jeffrey E Segall. Classifying collective cancer cell invasion. *Nature Cell Biology*, 14(8):777–783, 2012.

[2] Jacqueline D Shields, Mark E Fleury, Carolyn Yong, Alice A Tomei, Gwendalyn J Randolph, and Melody A Swartz. Autologous chemotaxis as a mechanism of tumor cell homing to lymphatics via interstitial flow and autocrine ccr7 signaling. *Cancer cell*, 11(6):526–538, 2007.

[3] Kevin J Cheung, Edward Gabrielson, Zena Werb, and Andrew J Ewald. Collective invasion in breast cancer requires a conserved basal epithelial program. *Cell*, 155(7):1639–1651, 2013.

[4] Andrew M Simons. Many wrongs: the advantage of group navigation. *Trends in ecology & evolution*, 19(9):453–455, 2004.

[5] Luke Coburn, Luca Cerone, Colin Torney, Iain D Couzin, and Zoltan Neufeld. Tactile interactions lead to coherent motion and enhanced chemotaxis of migrating cells. *Physical biology*, 10(4):046002, 2013.

[6] David Ellison, Andrew Mugler, Matthew Brennan, Sung Hoon Lee, Robert Huebner, Eliah Shamir, Laura A Woo, Joseph Kim, Patrick Amar, Ilya Nemenman, Andrew J Ewald, and Andre Levchenko. Cell-cell communication enhances the capacity of cell ensembles to sense shallow gradients during morphogenesis. *arXiv preprint arXiv:1508.04692*, 2015.

[7] Howard C Berg and Edward M Purcell. Physics of chemoreception. *Biophysical journal*, 20(2):193, 1977.

[8] William Bialek and Sima Setayeshgar. Physical limits to biochemical signaling. *Proceedings of the National Academy of Sciences of the United States of America*, 102(29):10040–10045, 2005.

[9] Kazunari Kaizu, Wiet de Ronde, Joris Paijmans, Koichi Takahashi, Filipe Tostevin, and Pieter Rein ten Wolde. The berg-purcell limit revisited. *Biophysical journal*, 106(4):976–985, 2014.

[10] Brendan A Bicknell, Peter Dayan, and Geoffrey J Goodhill. The limits of chemosensation vary across dimensions. *Nature communications*, 6, 2015.

[11] Alexandra Jilkine and Leah Edelstein-Keshet. A comparison of mathematical models for polarization of single eukaryotic cells in response to guided cues. *PLoS Comput Biol*, 7(4):e1001121–e1001121, 2011.

[12] Robert G Endres and Ned S Wingreen. Accuracy of direct gradient sensing by single cells. *Proceedings of the National Academy of Sciences*, 105(41):15749–15754, 2008.

[13] Robert G Endres and Ned S Wingreen. Accuracy of direct gradient sensing by cell-surface receptors. *Progress in biophysics and molecular biology*, 100(1):33–39, 2009.

[14] Bo Hu, Wen Chen, Wouter-Jan Rappel, and Herbert Levine. Physical limits on cellular sensing of spatial gradients. *Physical review letters*, 105(4):048104, 2010.

[15] Andrew Mugler, Andre Levchenko, and Ilya Nemenman. Limits to the precision of gradient sensing with spatial communication and temporal integration. *arXiv preprint arXiv:1505.04346*, 2015.

[16] Andre Levchenko and Pablo A Iglesias. Models of eukaryotic gradient sensing: application to chemotaxis of amoebae and neutrophils. *Biophysical journal*, 82(1):50–63, 2002.

[17] Alexandre J Kabla. Collective cell migration: leadership, invasion and segregation. *Journal of The Royal Society Interface*, page rsif20120448, 2012.

[18] A Szabó, R Ünnep, E Méhes, WO Twal, WS Argraves, Y Cao, and A Czirók. Collective cell motion in endothelial monolayers. *Physical biology*, 7(4):046007, 2010.

[19] Markus Basan, Jens Elgeti, Edouard Hannezo, Wouter-Jan Rappel, and Herbert Levine. Alignment of cellular motility forces with tissue flow as a mechanism for efficient wound healing. *Proceedings of the National Academy of Sciences*, 110(7):2452–2459, 2013.

[20] Albertas Janulevicius, Mark van Loosdrecht, and Cristian Picioreanu. Short-range guiding can result in the formation of circular aggregates in myxobacteria populations. *PLoS Comput Biol*, 11, 2015.

[21] Brian A Camley, Juliane Zimmermann, Herbert Levine, and Wouter-Jan Rappel. Emergent collective chemotaxis without single-cell gradient sensing. *arXiv preprint arXiv:1506.06698*, 2015.

[22] Roberto Mayor and Carlos Carmona-Fontaine. Keeping in touch with contact inhibition of locomotion. *Trends in cell biology*, 20(6):319–328, 2010.

[23] François Graner and James A Glazier. Simulation of biological cell sorting using a two-dimensional extended potts model. *Physical review letters*, 69(13):2013, 1992.

[24] Athanasius F. M. Marée, Verônica A. Grieneisen, and Paulien Hogeweg. The Cellular Potts Model and Biophysical Properties of Cells, Tissues and Morphogenesis. In Alexander R. A. Anderson, Mark A. J. Chaplain, and Katarzyna A. Rejniak, editors, *Single-Cell-Based Models in Biology and Medicine*, Mathematics and Biosciences in Interaction. Birkhäuser Basel, 2007. DOI: 10.1007/978-3-7643-8123-3_5.

[25] Maciej H Swat, Gilberto L Thomas, Julio M Belmonte, Abbas Shirinifard, Dimitrij Hmeljak, and James A Glazier. Multi-scale modeling of tissues using compucell3d. *Methods in cell biology*, 110:325, 2012.

[26] Oliver J Maclaren, AG Fletcher, HM Byrne, and Philip K Maini. Models, measurement and inference in epithelial tissue dynamics. *arXiv preprint arXiv:1506.05052*, 2015.

[27] Bongseop Kwak, Altug Ozcelikkale, Crystal S Shin, Kinam Park, and Bumsoo Han. Simulation of complex transport of nanoparticles around a tumor using tumor-microenvironment-on-chip. *Journal of Controlled Release*, 194:157–167, 2014.

[28] Crystal S Shin, Bongseop Kwak, Bumsoo Han, and Kinam Park. Development of an in vitro 3d tumor model to study therapeutic efficiency of an anticancer drug. *Molecular pharmaceutics*, 10(6):2167–2175, 2013.